Supporting Information

Kemp et al. 10.1073/pnas.1015619108

SI Text

Reconstructing Relative Sea Level in North Carolina and Massachusetts. In North Carolina, a modern dataset of 193 surface samples collected from 10 salt marshes (1) was used to develop transfer functions to quantify the relationship between foraminifera and elevation (2). We used these transfer functions to estimate paleomarsh elevation (PME) at Sand Point and Tump Point, North Carolina. PME is the elevation at which a sample formed with respect to its contemporary sea level (3). Foraminifera preserved in 1 cm thick samples from the Sand Point and Tump Point cores provided the basis for estimating PME. To reconstruct relative sea level (RSL), estimated PME was subtracted from the measured altitude of each sample. Core-top elevations were established by leveling to geodetic benchmarks (Sand Point) and Real Time Kinematic (RTK) satellite navigation (Tump Point), thus sample altitude was derived from depth-in-core measurements. Foraminifera and PME estimates for the Sand Point and Tump Point cores are presented in Fig. 1. Transfer functions provide error estimates that are unique to each sample (4). Uncertainty from sampling (e.g., angle of bore hole, sample thickness, RTK error) was minimal and not included in the vertical sea-level errors.

At Wood Island (Massachusetts), salt-marsh plants were used as sea-level indicators (5). The modern mean elevation of *Juncus geradii* (Jg), *Spartina patens* (Sp), and *Distichlis spicata* (Ds) was estimated by measuring stands at the Wood Island site. Multiple, stratigraphically ordered, samples were recovered along the boundary between a gently sloping granite erratic and overlying salt-marsh sediments. Identifiable remains of Jg, Sp, and Ds were used to provide an estimate of PME (Fig. S1).

Developing Composite Chronologies for North Carolina and Massachusetts. Original dating results for North Carolina and Massachusetts are provided in a separate file. A separate chronology was developed for the Sand Point and Tump Point cores, which were not combined or used to constrain one another in any way. The uppermost part of both cores was dated using a ^{210}Pb-derived accumulation history. Sample ages were estimated using the constant supply constant flux model (6), which was independently corroborated by a ^{137}Cs peak (corresponding to AD 1963) and bomb-spike ^{14}C dates. Material prepared for bomb-spike ^{14}C dating was analyzed using Accelerator Mass Spectrometry (AMS) with 15 repeats of 30,000 counts. Multiple samples were dated to facilitate calibration using the Northern Hemisphere Zone 2 dataset of Reimer et al. (7). High-precision ^{14}C ages (8) were obtained by preparing duplicate or triplicate samples from the same depth interval and using a pooled mean (Calib 5.0.1 software program) for calibration. Radiocarbon activity was determined from 15 repeats of 30,000 counts to improve instrument-related precision. Calibration was undertaken using Calib 5.0.1, reported errors are 2σ. An additional 15 samples at Sand Point and 7 at Tump Point were dated using conventional AMS ^{14}C. Calibration was undertaken using Calib 5.0.1, reported errors are 2σ. All samples were prepared for radiocarbon dating by cleaning under a binocular microscope to remove contaminating material. A pollen chronohorizon was identified in the Sand Point core by an increase in *Ambrosia* to 2% of total pollen, this change is indicative of land clearance during European settlement and was assigned an age of AD 1720 ± 20 y (9).

The discreet dated samples from Sand Point and Tump Point were used to generate a probabilistic age-depth model for each of the cores separately using the statistical package *Bchron* (10) executed in *R*. This approach used many thousands of iterations of the available data to provide an age-depth model with 95% confidence. This model was subsequently used to estimate the age (with a unique uncertainty) of every 1 cm thick sample in both cores, including those that were not directly dated. The uncertainty associated with estimating the age of individual 1 cm thick intervals ranged from ± 1 y (minimum) to ± 193 y (maximum), although more than 95% of samples had uncertainty of less than ± 71 y. In general, the smallest chronological errors were in the uppermost sections of each core (most recent), where age was constrained by techniques (^{210}Pb, ^{137}Cs, bomb-spike ^{14}C, and a pollen chrono-horizon) with small error terms. The chronologies (dates and age-depth models) for the Sand Point and Tump Point cores are presented in Fig. 1.

In Massachusetts, each of the samples used for estimating PME was also dated. 14 of the plant macrofossil samples were directly dated using AMS ^{14}C. Pollen evidence of European land clearance (AD 1700 in this region) and the chestnut decline (AD 1930) were used to estimate the age of two samples. A peak in ^{137}Cs associated with above ground testing of nuclear weapons was assigned an age of AD 1963 and an industrial horizon (AD 1875) was recognized by increased Pb and Cu concentrations and the occurrence of opaque spherules. The stratigraphical relationship between samples was used manually to better constrain the chronology derived from calibrated ^{14}C ages and reduce uncertainty. The dates and age model for the Wood Island site are presented in Fig. S1. The elevation-depth model, developed using *Bchron* (10), supports the manual constraint of the chronology.

All sea-level data points are represented by boxes incorporating the elevational and chronological uncertainties associated with individual samples. This data is presented in Table S1 for North Carolina and for Massachusetts. Reconstructed sea level from the Sand Point and Tump Point cores for the last ~400 y was presented by Kemp et al. (2). However, the data presented here spanning the last 400 y improve upon the existing record by introducing additional foraminiferal counts and new, statistically rigorous age-depth models developed using a newer technique.

In the main manuscript the data points reconstructing sea level in North Carolina are summarized using a 9 degree polynomial with 1σ and 2σ errors used to create a sea-level envelope which we have presented in pink. The purpose of this envelope is solely to provide a convenient visual summary of the data to aid the reader. The polynomial summary was not used for analysis of sea-level change in North Carolina.

Estimating Vertical Land Movements Associated with Glacial Isostatic Adjustment (GIA). Reconstructions of relative sea level are the net result of eustatic, isostatic, tectonic, and local factors. We assumed the tectonic factor to be zero in North Carolina and agreement between reconstructions from Sand Point and Tump Point (120 km apart) suggested that local factors were not a major influence. By assuming that the eustatic contribution to sea-level change over the last 2000 y was minimal (11), late Holocene sea-level reconstructions can be used to estimate the rate of GIA. A zero late Holocene sea-level eustatic function is a feature of most GIA models (12–14).

We used a standardized database of sea-level reconstructions collated for the US Atlantic coast to estimate the rate of GIA in North Carolina (15, 16). All data points that were not of base of basal or basal origin were excluded to negate the influence of sediment consolidation. Linear regression of the sea-level data points over the last 2000 y (excluding changes since AD 1900) estimated the rate of GIA to be 1.00 ± 0.03 mm/y in the region of Sand Point and 0.90 ± 0.02 mm/y at Tump Point. This uncertainty is the 2σ error of the regression line. Linear regression of midpoint sea-level reconstructions is appropriate for estimating rates of GIA in regions with sea-level histories constrained by a large number of data points with small age and vertical errors such as North Carolina (16). Model predictions support the use of a single linear rate of GIA over the late Holocene given Earth's rate of viscoelastic response (12–14). Predictions specifically for the areas around Sand Point and Tump Point show linear GIA for the last 2000 y (15). According to Engelhart et al. (16), there is 95% confidence that estimated rates of GIA (using this method) over the last 4000 y in North Carolina were within 0.10 mm/y of the values we have applied. GIA uncertainty has a propagating effect when used to adjust geological data because it becomes increasingly large further back in time. We did not include this effect as a stochastic error in our sea-level reconstruction (Figs. 2 and 3), but visually illustrate its influence by conservatively assuming a GIA uncertainty of ± 0.15 mm/y in Fig. 4.

Direct comparison among sea-level records is facilitated by correcting sea-level reconstructions for the effect of GIA. Uncertainty in estimating rates of GIA is therefore a possible cause for differences among records. All sites required correction for GIA. However, the location of a sea-level reconstruction (near, intermediate, or far field) does not influence the uncertainty of estimated GIA only its absolute value. In fact, uncertainty is proportionally less at sites experiencing high rates of GIA. Regional estimates of GIA have been derived from geological data or model predictions. Uncertainty is therefore dependent upon the quality of available geological data or the accuracy of model predictions which themselves have often been calibrated using sea-level data. The US Atlantic coast has one of the most detailed records of late Holocene sea level and sufficient, quality controlled data exists to identify to identify regional GIA trends with confidence.

The rate of GIA for Wood Island and Revere, Massachusetts (0.4 mm/y) and Barn Island (5), Connecticut (1 mm/y) was estimated using the same approach as described for North Carolina. In Figure 3, all sea-level records presented have had estimated GIA removed. Other published studies of late Holocene sea-level change were adjusted for rates of glacio-isostatic adjustment (GIA) using estimates presented in the original publication [Maine (17), Nova Scotia (17, 18), Louisiana (19), Iceland (20), Israel (21)), Italy (22), and the Cook Islands (23)], or from ref. 24 in the cases of Spain and New Zealand. No GIA correction was applied to the Israel data as the original publication states that the net effect was zero (21) because the rate of land subsidence was offset by ocean basin subsidence. In the Cook Islands, GIA is solely from subsidence of the ocean basin (23). In each example, except the record from Connecticut (25), sea-level data (and associated errors) were taken directly from the original publication or kindly provided by the author.

Estimating Rates of Sea-Level Change. Following adjustment for rates of GIA, we estimated rates of sea-level change for North Carolina. The datasets from Sand Point and Tump Point were only merged after this adjustment, by combining the age and sea-level estimates associated with individual data points into a single list. The sea-level data for North Carolina is complex because it consists of a large number of data points that are not spaced at regular temporal intervals and each of which has unique vertical and age uncertainties with an associated error distribution. Given the nature of the data, we used Bayesian change-point linear regression (26) to objectively and quantitatively identify discrete periods of GIA-adjusted sea-level change in North Carolina. We used the GIA-adjusted sea-level data points in this analysis and not the summary polynomial sea-level curve (Figs. 2, 3, and 4). This technique is able to provide probabilistic estimates of rates and the timings of rate changes in complex data following many thousands of iterations. Three change-points gave a good fit to the data by providing four successive segments of sea-level change, each of which was described by a linear rate of change. The regression was forced through zero because RSL must equal zero at the time of core collection. The model takes account of calibrated radiocarbon uncertainty by approximating each calibrated age as a normal distribution; it also takes into consideration vertical errors.

This technique provides a most likely sea-level history given the distribution of the data points and the distribution of uncertainties within them. The fitted lines represent mean, long-term, sea-level change rates and have 95% upper and lower confidence intervals. The model is necessarily an approximation, as each of the four segments is linear, and changes are instantaneous rather than gradual. For the North Carolina reconstruction, sea level prior to the first change-point (AD 853–1076) was between −0.03 and +0.06 mm/y (95% confidence). From here until the second change-point (AD 1274–1476) sea level rose at 0.37–0.80 mm/y (95% confidence interval). The third segment, until a change-point at AD 1865–1892, showed sea-level change of −0.16 to +0.02 mm/y (95% confidence). Since this most recent change-point sea level has risen at a rate of 1.90–2.20 mm/y (95% confidence interval). These ranges represent the uncertainty in fitting a single best fit change-point regression through the proxy data. However, due to the age and vertical errors in the proxy sea-level data, shorter-lived sea-level changes (particularly at subcentennial time scales) exceeding the rates described can be accommodated. Indeed, any sea-level history is permissible with the confines of the error boxes although the results from change-point linear regression suggest that they are less likely than the sea-level changes we described.

Bayesian change-point analysis was not applied to the Massachusetts data (or other reconstructions of sea level as presented in Fig. 3) because of temporal gaps in the record of up to 400 y. We calculated a GIA-adjusted value of sea-level change during the 20th century from the mid points of AD 1899 (RSL = 0.24 ± 0.04 m) and AD 2004 (RSL = 0 ± 0.04 m).

Validating Sea-Level Reconstructions Using Tide-Gauge Records. Instrumental records of sea-level variability provide a unique opportunity to independently check proxy-based reconstructions. Tide-gauge measurements are commonly averaged to reduce one year of data to a single point. Gauges with more than 50 y of data are considered to be the most representative of sea-level trends as the influence of annual-decadal scale variability is minimized (14, 16, 27). The distribution of such gauges is strongly biased toward the northern hemisphere. The longest tide-gauge records (such as Amsterdam, Liverpool, Brest, and Stockholm) are located in northern Europe (28, 29).

Sea-level reconstructions from salt marshes are developed using 1 cm thick slices of sediment from core material. The effect of this approach is twofold. Firstly, sea-level indicators on salt marshes such as plants and foraminifera do not respond to short-lived variability in sea level. Secondly, the 1 cm slices of sediment represent a period of time, which is dependent on the rate of sediment accumulation, but is on the order of years. Both of these factors serve to make salt marshes excellent archives of persistent paleo sea-level trends because short-lived and annual variability is naturally filtered out. Therefore it is unreasonable to expect sea-level reconstructions to resolve sea-level changes with the same resolution as tide gauges. In fact, this filtering means it is often easier to extract sea-level trends from salt marshes than from noisy tide-gauge records.

We consider reconstructed sea level to be in agreement with tide-gauge measurements when persistent trends can be seen in both records and where tide-gauge measurements pass though sea-level reconstruction boxes incorporating age and vertical uncertainties. In Fig. 2*B* we show that tide-gauge data with annual resolution from North Carolina (since AD 1936) and Charleston, South Carolina (since AD 1920) are in agreement with the sea-level reconstructions from Sand Point and Tump Point. Compilations of tide-gauge records with global significance (28, 29) have recently been extended to AD 1700. In Fig. 3 we show that there is excellent agreement among these records and reconstructed sea level in North Carolina. For the period since AD 1880 the record of Church et al. (30) does not leave the summary sea-level envelope constructed for North Carolina and at no point does the midpoint of the Jevrejeva et al. record (28) covering the period since AD 1700 leave this envelope (Fig. 3). In Fig. S6 we compare the North Carolina sea-level reconstruction to the global tide-gauge-compilation of ref. 28, where the tide-gauge data was summarized using change-point regression. The largest difference between the two datasets was 6 cm which is less than the uncertainty for the North Carolina reconstruction and much of the tide-gauge data. This agreement provides confidence that salt marshes in North Carolina provide accurate reconstructions of long-term, persistent changes in sea level during the late Holocene.

High-Resolution Numerical Modeling of Tidal-Range Change from Barrier Breaching in the Albemarle–Pamlico Estuarine System of North Carolina. If tidal range has changed through time, sea-level reconstructions based upon tide-level indicators will differ from the "true" sea-level curve. To investigate this influence for Sand Point and Tump Point we modeled the influence of barrier breaching on tidal range using the Advanced Circulation Model for Coastal Ocean Hydrodynamics (ADCIRC). The open boundary of the grid was forced with six tidal constituents and runs were carried out for 60 d of model time, with a 10 d ramp. The final 45 d of the simulations were used to perform a harmonic analysis of the results. This harmonic analysis yielded the amplitudes and phases of 23 tidal constituents. In turn, these constituents were used to determine major tidal datums, such as mean higher high water (MHHW), mean lower low water (MLLW). Tidal range was taken to be the difference between MHHW and MLLW. The modeled study area covered the Outer Banks area of North Carolina from Bogue Inlet in the south to the border of North Carolina and Virginia in the north. In this region there are currently six inlets. From north to south these are: Oregon Inlet, Hatteras Inlet, and Ocracoke Inlet, which lead into Pamlico Sound; Drum Inlet and Barden Inlet (at Cape Lookout), which lead into Core Sound; Beaufort Inlet and Bogue, which lead into Bogue Sound. The tidal range on the ocean-side of the Outer Banks ranges from about 0.75 m to 1.25 m. Once the tide propagates through the northern inlets, it is quickly damped in Pamlico and Albemarle Sounds to a range that is less than 0.25 m and in many places less than 0.15 m. In Core, Back, and Bogue Sounds, tidal range is lower than on the ocean-side of the Outer Banks, but ranges from 0.25 m to 1.1 m.

Small inlet breaches. For this study, eight additional inlets were added to the model domain. Each of these new inlets was set to an approximate center depth of 6 m. As with existing inlets, tidal range declined rapidly after the tide propagated through the inlets. Increasing the number of inlets caused tidal range at our study sites to increase on the order of 0.05 m, within the uncertainty band shown for our analysis.

Large inlet breaches. To simulate "catastrophic" collapse of the barrier islands, six huge sections of the Outer Banks were removed. The bathymetry that existed in the original grid on either side of the barrier islands was kept, and simply interpolated between these two to create a new depth in the area where the island was supposed to have collapsed. The results from the model simulations show tidal range increases in the sound area. There was significant spatial variability, with larger increases near to Tump Point, and lower increases toward the Pamlico and Neuse River inlets, near the Sand Point site. These differences in tidal range would produce RSL reconstructions from Sand Point and Tump Point that would be different to one another. But the records have near identical sea-level variations. This agreement suggests that tidal-range change was not an important influence on sea level in the region over the past two millennia.

Ice Sheet Gravity Effect on the Proxy Sea-Level Data. In addition to the effect of GIA since the last deglaciation, there is also the gravity effect on the geoid of shrinking continental ice sheets, and thus on local sea level. This phenomenon causes local rates of sea-level rise to differ from the global average and has been termed fingerprinting (31). The values found by Mitrovica et al. (31) are provided in Table S2, for two different GIA modeling approaches. The first approach uses, as they explain, "the combination of ice and Earth models adopted in a number of earlier studies;" the second uses a modified GIA model, where lower mantle viscosity is increased from 2×10^{21} to 5×10^{21} Pa s (Pascal seconds), in order to better fit historical tide-gauge data along the US Atlantic coast (Table S2).

The "fingerprint" of sea-level rise in North Carolina due to melting of the Greenland Ice Sheet, defined as local sea-level rise expressed as a fraction of global average sea-level rise from this source, is 60% (from Fig. 1*B* in ref. 31). For small glaciers, the fingerprint is 95% (from Fig. 1*C* in ref. 31). If we assume a fingerprint of 100% for both Antarctica and "other" (mainly thermosteric rise), we find that the *total* sea-level rise in North Carolina, computed using the above tabulated contributions as weights, is 87% and 83% respectively under the two GIA scenarios (see Fig. 1*A* in ref. 31).

As there is no guarantee that relative contributions from the various continental ice sheets to sea-level rise have been constant over time, it is not feasible to correct the North Carolina record for this effect because the uncertainties are too great. We restrict ourselves here to a sensitivity study, where we assume local sea-level rise to be 83% of the global average (i.e., we multiply North Carolina sea-level values by $1/0.83 = 1.2$) to compare with sea-level curves reconstructed from the temperature proxy data. This exercise is depicted in Fig. S2. It is seen that even a worst-case fingerprint effect of 83% leads only to a barely (if at all) visible deterioration of the quality of fit.

Assumed Prior Information. We assumed the statistics summarized in Table S2 for the reconstructed temperatures, model fit parameters, and integration constants.

Bayesian Updating to Estimate the Model Parameters. We used Bayes' theorem in the following form:

$$P(\theta|x) = (P(x|\theta)/P(x))P(\theta) = L_x(\theta)P(\theta),$$

where we defined the likelihood function as

$$L_x(\theta) = \prod_{i=1}^{n} \exp((-1/2)(H(t_i;\theta) - H_i)^2/\sigma^2),$$

where H_i is a proxy-reconstructed sea-level value, $\theta = \{\tau, a_1, a_2, H_0, \langle T_0 \rangle, T_0(\mathrm{AD500}), T(t)\}$ is the unknown parameter vector for which our Bayesian update will produce a probability density distribution, and $H(t_i;\theta)$ is sea level as predicted from temperature by our relationship for the epoch t_i. Standard error (σ) is the formal uncertainty of the n sea-level proxy data points. H_0 and $T_0(\mathrm{AD\,500})$ are integration constants of Eq. 2.

Note that the above equation describes the goodness by which an individual sea-level curve as predicted by our relationship from a Monte Carlo generated temperature curve "fits through" the observed sea-level points H_i. Thus, in the Bayesian update step this quantity is used to update the a posteriori probability of this curve among the generated ensemble. These probabilities, for all ensemble members, are then used to generate a posteriori uncertainty bands.

The result of the Bayesian prediction is somewhat dependent on the choice of weighting for the sea-level proxy data; it is necessary to downweight them (or inflate their assumed variance) to take into account that they are subject to strong serial correlation. An appropriate choice for this factor would be 10. With this choice, we find it is not possible to obtain a reasonable a posteriori result for the entire data period: it is necessary to exclude the sea-level data before AD 1000 from the fit.

Fig. 5 shows the resulting probability density distributions for the unknown parameters and functions of interest, and some correlation point clouds. One sees that parameter a_1 is constrained to 0–0.25 cm/K/y, and τ to 0–1000 y, with likely values in the 100–500 y range.

Computation and Plotting Details. We generated the medial curves and uncertainty bands displayed in our plots in the following way. For plots marked a priori, we generated 1,000 samples, for plots marked a posteriori, 25,000 samples. The plotted curves were smoothed using Singular Spectrum Analysis (SSA) smoothing (32) with an "embedding dimension" of 15 y, compatible with Vermeer and Rahmstorf (33). A polynomial was fitted to the North Carolina sea-level reconstruction and was used as a visual summary of the data. A 9 degree polynomial (as opposed to one of higher or lower order) was used because it captured the main features of reconstructed sea-level behavior at the time scales we resolve. Raising the degree only marginally improved fit to the data.

Both temperatures and sea levels were plotted relative to a reference level equal to the average for the period AD 1400–1800 [for the Mann et al. (34) reconstructed temperatures and the North Carolina reconstructed sea levels, respectively], corresponding with a reasonable notion of "preindustrial." In the plots, the reconstructed North Carolina sea levels are represented by a red curve with pink 1σ and 2σ uncertainty bands, cut away for visibility where appropriate.

The values of a_1 and $T_{0,0}$. From the plots in Fig. 5 (in particular, the two bottom right ones) it is seen that, while a_1 and $T_{0,0}$ are not separately strongly constrained, nevertheless the product $-a_1 \bullet T_{0,0}$ is constrained, and positive. As a_1 approaches zero from above, $T_{0,0}$ approaches minus infinity. This behavior is a direct consequence of the compatibility condition (35)

$$aT_0 = a_1 T_{0,0} + a_2 \langle T_0 \rangle$$

with the parameters found from the fit to the instrumental period (33). Our results thus suggest a positive value for the secular part of sea-level rise today.

Weighting and fit for the early period (AD 500–1100). To fit the sea-level proxy data back to AD 500 required down-weighting of the data and generated an inadequate fit with broad uncertainty bands, suggesting that the data is not compatible. Restricting the Bayesian update to only post-AD 1000 sea-level data markedly improved the fit (Fig. 3*D*), but increased divergence between sea-level proxy data and sea-level predicted prior to AD 1000. There is independent evidence (21, 22) that the steep sea-level rise predicted from temperatures between AD 500 and 1000 is unphysical, and thus that the sea-level proxy data from North Carolina for this period are more realistic. This conclusion is supported by sea-level reconstructions from Massachusetts (36) and elsewhere (16, 37).

Lowering reconstructed temperature by 0.2 K for the period AD 500–1100 produced good agreement with the North Carolina sea-level reconstruction (Fig. S4). We studied the sensitivity of this fit to a range of temperature corrections (−0.1 K to −0.3 K). As shown in Fig. S5, the best agreement was for a −0.2 K correction. An error of this magnitude is not implausible as we used the global Mann et al. (34) reconstruction prior to AD 1100 and not the Northern-Hemisphere-only reconstruction in which Mann et al. (34) had greater confidence. For the period prior to AD 1100, availability of proxy temperature reconstructions is poor for the Southern Hemisphere and this is necessarily reflected in greater uncertainty for global estimates which can accommodate a 0.2 K reduction in temperature within their uncertainty. This reduction in reconstructed temperature would make the Medieval Climate Anomaly globally less pronounced than Mann et al. (34) suggested, and reduce by a half its temperature contrast with the Little Ice Age.

An alternative explanation is that reconstructed sea level is in error. This reasoning does not appear credible because no other sea-level reconstruction suggests a stronger sea-level rise before AD 1100 (Fig. 3), as warm temperatures would imply under our semiempirical model. More rapid sea-level rise prior to AD 1100 would be a feature of predicted sea level using the Mann et al. (34) global temperature record and our semiempirical model regardless of the correction made for GIA. Further, agreement between the Sand Point and Tump Point records, despite differences in accumulation history and being more than 100 km apart suggests that local-scale factors were not important influences on RSL.

While the Grinsted et al. (38) prediction of former sea level is somewhat similar to ours, it features large sea-level variations (greater than 0.5 m) during the last 2000 y (see Fig. S6). The magnitude of these predicted sea-level changes is dependent on the temperature reconstructions used as input and their uncertainties. Only for the post- AD 1700 period, for which Grinsted et al. (38) used tide-gauge data from northwestern Europe to calibrate their model, is there a good agreement with our result. This agreement implies that these extended tide-gauge records are representative of former sea level.

Performance over the instrumental period. We tested the performance of our relationship over the instrumental period, AD 1880–2000 (Fig. 6). For temperatures, taken from Mann et al. (34), this is essentially a test of the HadCRUTv3 temperature dataset. For instrumental sea level, we took Church and White (29), with an estimated contribution due to the artificial reservoir effect added as described in ref. 33.

Loose parameter constraints. We also produced a reconstruction in which we did not use the prior constraints on the parameters from ref. 33. Instead, we used the following, loose constraints, effectively producing near-ignorant priors:

$$a = 0.44 \pm 0.5 \text{ cm/K/yr}$$

$$b = 0 \text{ (exactly)}$$

$$T_0(\text{AD } 1880\text{–}2000) = -0.45 \pm 0.3 \text{ K}.$$

Furthermore we loosened the constraint of the integration constant H_0 to be $U(-10 \text{ cm}, 10 \text{ cm})$. The reason for fixing b was, that it is not possible to simultaneously solve for a and b using only the paleo data, as we found this to be an ill-posed problem. Fixing b to another value will only change the value obtained for a and not produce any other significant changes to the solution.

For this run we used a sample size of 250,000 instead of the usual 25,000. We found the following posteriors:

$$a = 0.60 \pm 0.15 \text{ cm/K/yr}$$

$$-a_1 \bullet T_{0,0} = 0.139 \pm 0.043 \text{ cm/yr}$$

$$\ln(\tau) = 5.83 \pm 0.78[\tau \text{ in years}].$$

From Fig. S3 we see that τ is still robustly constrained to be finite. Also, remarkably, $-a_1 \bullet T_{0,0}$, a measure for long-term (intermillennial) sea-level rise, is seen to be very likely positive. Note that coefficient a is resolved to a value even larger than is typically obtained from semiempirical fits to the instrumental period.

The reason for the somewhat larger a is that the 20th century rise in the North Carolina data is somewhat larger than that given by global sea-level reconstructions from instrumental data, as discussed in the paper. That is why our preferred modeled sea-level curve (Fig. 4*D*) was constrained with instrumental data after AD 1880. Also the fingerprint effect should be considered, correcting for which however would tend to make a larger still.

1. Kemp AC, Horton BP, Culver SJ (2009) Distribution of modern salt-marsh foraminifera in the Albemarle-Pamlico estuarine system of North Carolina, USA: implications for sea-level research. *Mar Micropaleontol* 72:222–238.
2. Kemp AC, et al. (2009) Timing and magnitude of recent accelerated sea-level rise (North Carolina, United States). *Geology* 37:1035–1038.
3. Edwards RJ (2007) *Sea-Level Studies: Low Energy Coasts Sedimentary Indicators. Encyclopedia of Quaternary Science*, ed Elias SA (Elsevier, Amsterdam), pp 2994–3005.
4. Birks HJB (1995) *Quantitative Palaeoenvironmental Reconstructions. Statistical Modelling of Quaternary Science Data*, Technical Guide, eds Maddy D, Brew JS (Quaternary Research Association, Cambridge), Vol Technical Guide 5, pp 161–254.
5. Donnelly JP, Cleary P, Newby P, Ettinger R (2004) Coupling instrumental and geological records of sea-level change: evidence from southern New England of an increase in the rate of sea-level rise in the late 19th century. *Geophys Res Lett* 31:L05203.
6. Appleby PG, Oldfield F (1992) *Application of Lead-210 to Sedimentation Studies. Uranium Series Disequilibrium: Applications to Environmental Problems*, eds Ivanovich M, Harmon RS (Clarendon Press), pp 731–778.
7. Reimer PJ, et al. (2004) IntCal04 terrestrial radiocarbon age calibration, 0–26 cal kyr BP. *Radiocarbon* 46:1029–1058.
8. Marshall WA, et al. (2007) The use of "bomb spike" calibration and high-precision AMS C-14 analyses to date salt-marsh sediments deposited during the past three centuries.*Quaternary Research* 68:325–337 (in English).
9. Cooper S, McGlothlin S, Madritch M, Jones D (2004) Paleoecological evidence of human impacts on the Neuse and Pamlico estuaries of North Carolina, USA. *Estuaries and Coasts* 27:617–633.
10. Parnell AC, Haslett J, Allen JRM, Buck CE, Huntley B (2008) A flexible approach to assessing synchroneity of past events using Bayesian reconstructions of sedimentation history. *Quaternary Sci Rev* 27:1872–1885.
11. Milne GA, Long AJ, Bassett SE (2005) Modelling Holocene relative sea-level observations from the Caribbean and South America. *Quaternary Sci Rev* 24:1183–1202.
12. Peltier WR (1996) Global sea-level rise and glacial isostatic adjustment: an analysis of data from the east coast of North America. *Geophys Res Lett* 23:GL00848.
13. Peltier WR (2002) On eustatic sea-level history: last glacial maximum to Holocene. *Quaternary Sci Rev* 21:377–396.
14. Douglas BC (1995) Global sea-level change: determination and interpretation. *Reviews of Geophysics* 33:1425–1432.
15. Horton BP, et al. (2009) Holocene sea-level changes along the North Carolina Coastline and their implications for glacial isostatic adjustment models. *Quaternary Sci Rev* 28:1725–1736.
16. Engelhart SE, Horton BP, Douglas BC, Peltier WR, Tornqvist TE (2009) Spatial variability of late Holocene and 20th century sea-level rise along the Atlantic coast of the United States. *Geology* 37:1115–1118.
17. Gehrels WR, Belknap DF, Black S, Newnham RM (2002) Rapid sea-level rise in the Gulf of Maine, USA, since AD 1800. *The Holocene* 12:383–389.
18. Gehrels WR, et al. (2005) Onset of recent rapid sea-level rise in the western Atlantic Ocean. *Quaternary Sci Rev* 24:2083–2100.
19. González JL, Törnqvist TE (2009) A new late Holocene sea-level record from the Mississippi Delta: evidence for a climate/sea-level connection? *Quaternary Sci Rev* 28:1737–1749.
20. Gehrels WR, et al. (2006) Rapid sea-level rise in the North Atlantic Ocean since the first half of the nineteenth century. *Holocene* 16:949–965.
21. Sivan D, et al. (2004) Ancient coastal wells of Caesarea Maritima, Israel, an indicator for relative sea-level changes during the last 2,000 years. *Earth Planet Sc Lett* 222:315–330.
22. Lambeck K, Anzidei M, Antonioli F, Benini A, Esposito A (2004) Sea level in Roman time in the Central Mediterranean and implications for recent change. *Earth Planet Sc Lett* 224:563–575.
23. Goodwin ID, Harvey N (2008) Subtropical sea-level history from coral microatolls in the Southern Cook Islands, since 300 AD. *Mar Geol* 253:14–25.
24. Peltier WR (2001) Global glacio-isostatic adjustment and modern instrument records of relative sea-level history. *Sea-level rise history and consequences*, eds Douglas BC, Kearney MS, Leatherman SP (Academic Press, San Diego).
25. van de Plassche O, van der Borg K, de Jong AFM (1998) Sea-level-climate correlation during the past 1,400 yr. *Geology* 26:319–322.
26. Carlin BP, Gelfand AE, Smith AFM (1992) Hierarchical Bayesian analysis of change-point problems. *Applied Statistics* 41:389–405.
27. Douglas BC (1991) Global sea-level rise. *J Geophys Res* 96:6981–6992.
28. Jevrejeva S, Moore JC, Grinsted A, Woodworth PL (2008) Recent global sea-level acceleration started over 200 years ago? *Geophys Res Lett* 35:L08715.
29. Church JA, White NJ (2006) A 20th century acceleration in global sea-level rise. *Geophys Res Lett* 33:L01602.
30. Church J, et al. (2008) Understanding global sea levels: past, present and future. *Sustainability Science* 3:9–22.
31. Mitrovica JX, Tamisiea ME, Davis JL, Milne GA (2001) Recent mass balance of polar ice sheets inferred from patterns of global sea-level change. *Nature* 409:1026–1029.
32. Moore JC, Grinsted A, Jevrejeva S (2005) New tools for analyzing the time series relationships and trends. *Eos Trans AGU* 86:226.
33. Vermeer M, Rahmstorf S (2009) Global sea-level linked to global temperature. *Proc Nat'l Acad Sci USA* 106:21527–21532.
34. Mann ME, et al. (2008) Proxy-based reconstructions of hemispheric and global surface temperature variations over the past two millennia. *Proc Nat'l Acad Sci USA* 105:13252–13257.
35. Rahmstorf S (2007) A semiempirical approach to projecting future sea-level rise. *Science* 315:368–370.
36. Donnelly JP (2006) A revised late Holocene sea-level record for northern Massachusetts, USA.*Journal of Coastal Research* 22:1051–1061 (in English).
37. Peltier WR (1996) Global sea-level rise and glacial isostatic adjustment: an analysis of data from the East Coast of North America. *Geophys Res Lett* 23:717–720.
38. Grinsted A, Moore J, Jevrejeva S (2009) Reconstructing sea-level from paleo and projected temperatures 200 to 2100 AD. *Clim Dynam* 34:461–472

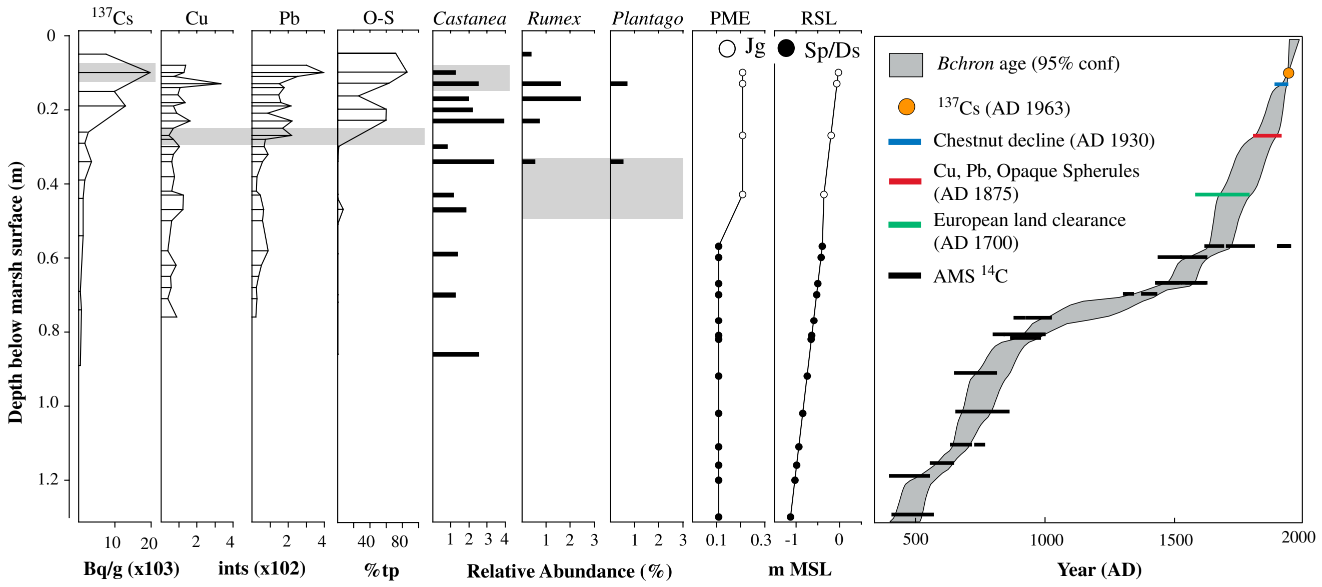

Fig. S1. Chronostratigraphy of the Wood Island (Massachusetts) site developed using AMS ^{14}C dating, heavy metal concentrations (Cu and Pb), opaque spherules (O-S), and pollen. Metal concentrations are presented as integrated peak area (ints), opaque sperhule abundance is expressed as a percentage of total pollen (%$_{tp}$). Paleo marsh elevation (PME) was estimated using plant macrofossils (Jg = *Juncus geradii*; Sp/Ds = *Spartina patens*; or *Distichlis spicata*). The modern distribution of these plants with respect to sea level was estimated by repeated leveling at the Wood Island site. Samples were collected from the sediment-erratic contact exposed by excavating a trench and are presented as depth below modern marsh surface. Chronological horizons are shown by gray shading.

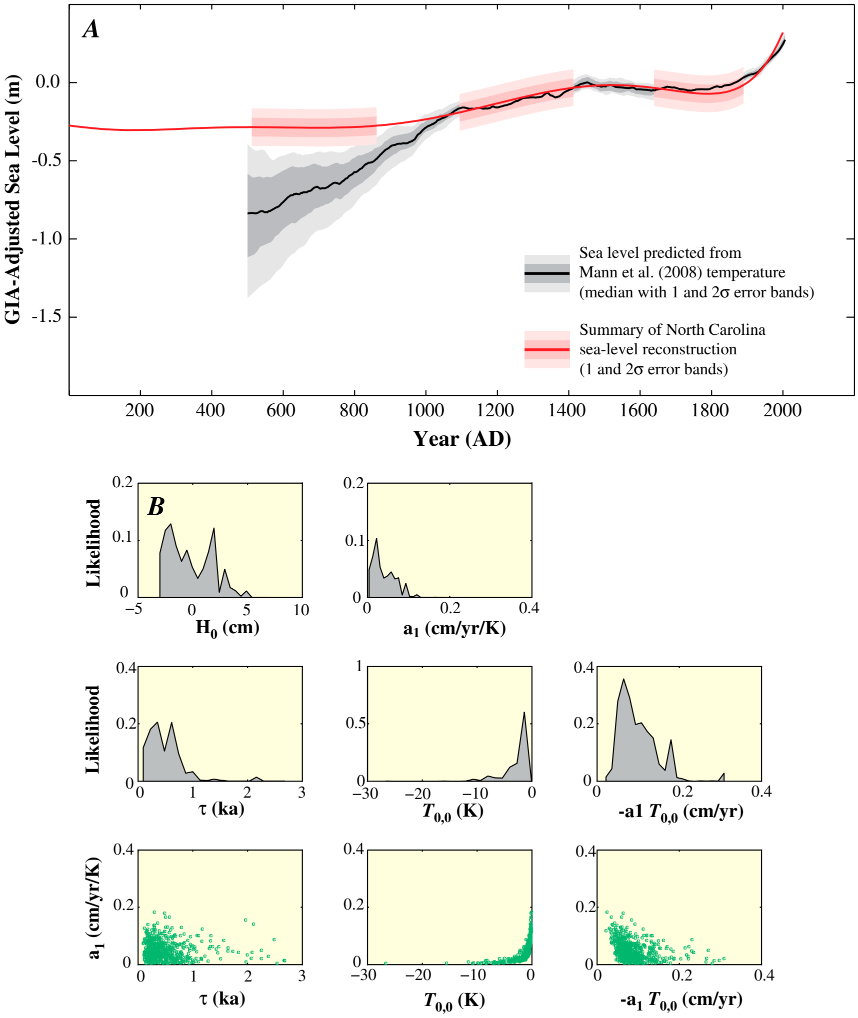

Fig. S2. Sensitivity analysis for the ice sheet gravity effect in North Carolina. Shrinking ice sheets distort the geoid causing local sea-level changes to differ from the global average. (*A*) Sea-level reconstruction from paleo-temperature (gray) and proxy-reconstructed sea levels from North Carolina with uncertainties as cutaway color bands (pink). Scaled for a fingerprint in which North Carolina experiences 83% of global sea-level rise (computed in Table S2). GIA-adjusted sea level is expressed relative to AD 1400–1800 average. (*B*) Posterior probability density distributions and correlation point clouds for selected quantities; ka is thousand years.

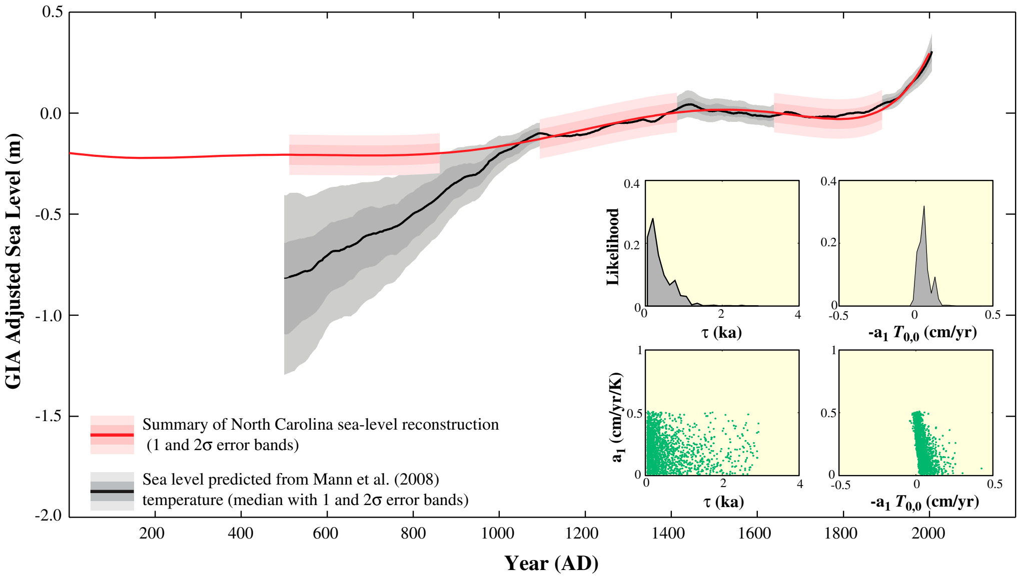

Fig. S3. Sea-level reconstruction (gray) for relaxed prior constraints on the parameters *a*, *b*, $\langle T_0(\text{AD } 1880–2000)\rangle$, and H_0, with histograms and scatter plots as insets. Proxy-reconstructed sea levels from North Carolina with uncertainties as cutaway color bands in pink. GIA-adjusted sea level is expressed relative to AD 1400–1800 average.

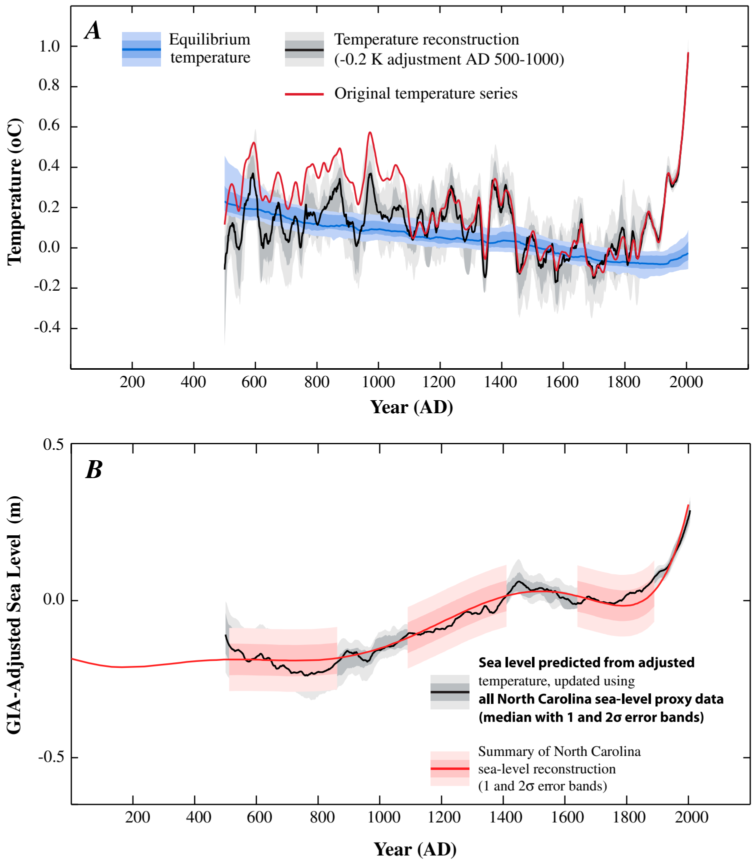

Fig. S4. Sea level predicted from paleo-temperature data, using sea-level proxy data from the whole period. Shaded error bands indicate 1σ and 2σ uncertainties. A correction of −0.2 K was applied to temperatures for AD 500–1100. (*A*) Temperature expressed relative to AD 1400–1800 average (gray; original from ref. 34 =red, reconstructed; median = black) and equilibrium temperature (blue). (*B*) Sea level predicted from adjusted temperature (gray) and summary of proxy-reconstructed sea levels from North Carolina (pink). GIA-adjusted sea level expressed relative to AD 1400–1800 average.

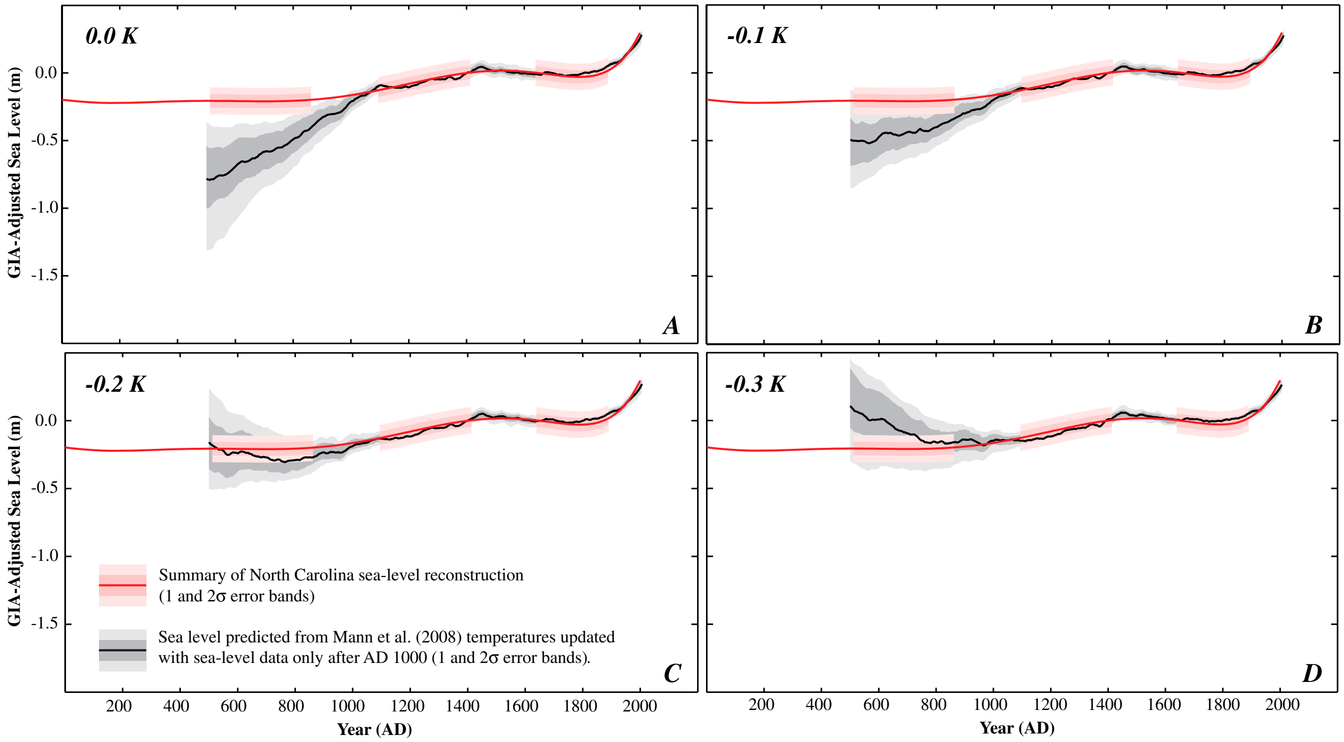

Fig. S5. The effect of amending reconstructed temperature for the period before AD 1100. Adjustments of (*A*) 0.0 K; (*B*) −0.1 K; (*C*) −0.2 K; and (*D*) −0.3 K were made to the composite error-in-variables land plus ocean global temperature reconstruction of Mann et al. (34). Proxy-reconstructed sea levels from North Carolina with uncertainties as cutaway color bands (pink). GIA-adjusted sea level is expressed relative to AD 1400–1800 averages.

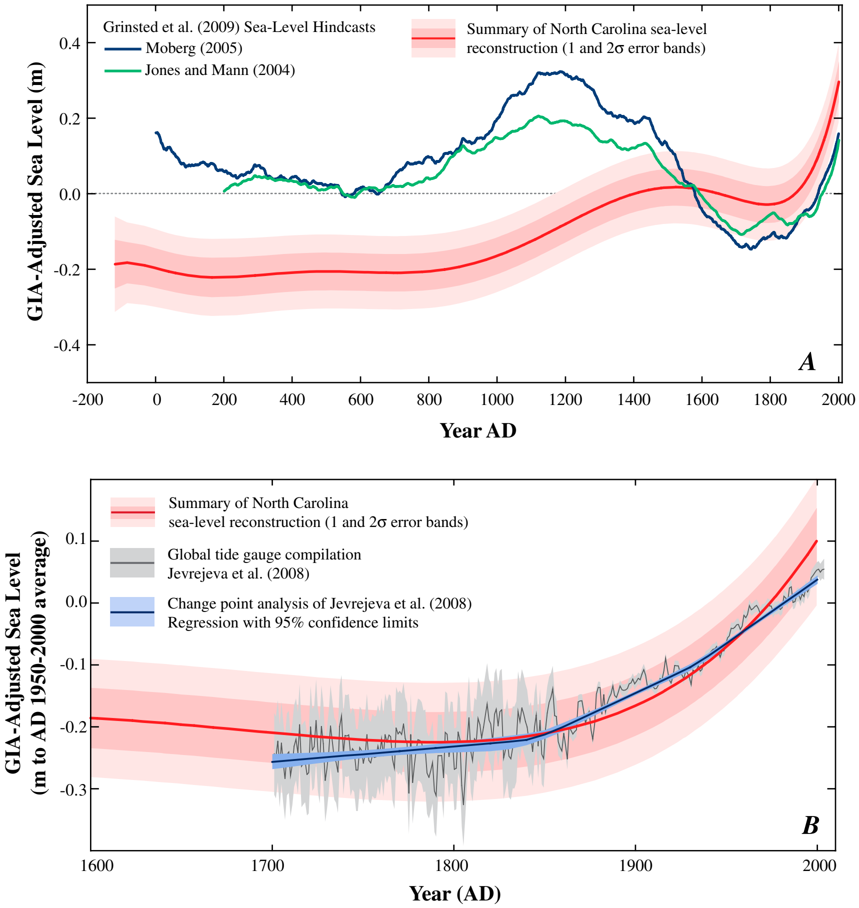

Fig. S6. (*A*) Comparison of reconstructed sea level from North Carolina (pink) and sea-level hindcasts from the semiempirical model of Grinsted et al. (1). Two reconstructions of climate (2, 3) were used to predict former sea level from the semiempirical model of Grinsted et al. (1). Uncertainties in sea-level hindcasts are not presented. Predictions using the Moberg dataset (2) were favored by Grinsted et al. (1). Sea level for each dataset is adjusted for GIA and expressed relative to AD 1400–1800 average. (*B*) Comparison of GIA-adjusted sea-level reconstruction from North Carolina (red, with pink error bounds) with the global tide-gauge-compilation (gray with error bounds) of Jevrejeva et al. (4). The tide-gauge data were summarized using change-point regression (blue, with 95% confidence interval). All series are shown relative to the average over the period AD 1950–2000.

1 Grinsted A, Moore J, Jevrejeva S (2009) Reconstructing sea-level from paleo and projected temperatures 200 to 2100 ad. *Clim Dynam* doi: 10.1007/s00382-00008-00507-00382.
2 Moberg A, Sonechkin DM, Holmgren K, Datsenko NM, Karlen W (2005) Highly variable Northern Hemisphere temperatures reconstructed from low- and high-resolution proxy data. *Nature* 433:613–617.
3 Jones PD, Mann ME (2004) Climate over past millennia. *Reviews of Geophysics* 42:2003RG000143.
4 Jevrejeva S, Moore JC, Grinsted A, Woodworth PL (2008) Recent global sea-level acceleration started over 200 years ago? *Geophys Res Lett* 35:L08715.

Table S1. Sea-level data points from North Carolina (Sand Point = SP and Tump Point = TP) and Wood Island Massachusetts. RSL = relative sea level

North Carolina

Year (AD/BC)	RSL (m)	Age error (yrs)	RSL error (m)	Site
2000	0.02	2	0.03	TP
1995	0.02	1	0.04	TP
1986	0.00	5	0.03	TP
1977	−0.01	4	0.03	TP
1977	−0.07	3	0.05	SP
1973	0.00	4	0.03	TP
1973	−0.11	3	0.05	SP
1969	−0.10	2	0.05	SP
1965	−0.16	2	0.05	SP
1961	−0.07	3	0.03	TP
1961	−0.18	2	0.05	SP
1959	−0.17	2	0.05	SP
1959	−0.07	2	0.03	TP
1957	−0.17	2	0.05	SP
1956	−0.08	2	0.03	TP
1948	−0.19	3	0.05	SP
1946	−0.16	5	0.03	TP
1944	−0.25	3	0.05	SP
1942	−0.17	3	0.09	SP
1940	−0.17	3	0.08	SP
1939	−0.18	5	0.03	TP
1938	−0.21	4	0.06	SP
1937	−0.22	4	0.07	SP
1935	−0.19	4	0.04	SP
1935	−0.15	5	0.03	TP
1934	−0.27	4	0.06	SP
1933	−0.23	5	0.05	SP
1931	−0.25	5	0.05	SP
1927	−0.21	6	0.03	TP
1926	−0.31	5	0.05	SP
1924	−0.24	6	0.03	TP
1922	−0.32	5	0.05	SP
1916	−0.26	6	0.03	TP
1915	−0.30	5	0.06	SP
1909	−0.31	7	0.04	TP
1909	−0.28	5	0.07	SP
1904	−0.32	6	0.06	SP
1903	−0.32	7	0.04	TP
1900	−0.34	8	0.04	TP
1890	−0.38	8	0.04	TP
1877	−0.35	22	0.05	SP
1877	−0.39	14	0.04	TP
1865	−0.40	18	0.03	TP
1852	−0.40	19	0.03	TP
1849	−0.39	35	0.06	SP
1840	−0.39	35	0.06	SP
1833	−0.46	18	0.04	TP
1831	−0.41	33	0.05	SP
1826	−0.46	16	0.03	TP
1822	−0.41	30	0.07	SP
1811	−0.42	25	0.06	SP
1793	−0.45	20	0.06	SP
1785	−0.43	21	0.03	TP
1777	−0.44	18	0.06	SP
1764	−0.47	24	0.06	SP
1760	−0.48	29	0.03	TP
1751	−0.50	27	0.05	SP
1739	−0.47	26	0.07	SP
1727	−0.54	33	0.03	TP
1726	−0.52	21	0.05	SP
1715	−0.53	33	0.03	TP
1697	−0.56	29	0.06	SP
1692	−0.56	29	0.03	TP
1676	−0.57	36	0.04	SP
1667	−0.57	26	0.03	TP
1657	−0.58	40	0.04	SP
1650	−0.62	28	0.03	TP

North Carolina

Year (AD/BC)	RSL (m)	Age error (yrs)	RSL error (m)	Site
1648	−0.59	40	0.04	SP
1641	−0.63	29	0.03	TP
1639	−0.59	40	0.05	SP
1629	−0.63	38	0.06	SP
1623	−0.64	28	0.03	TP
1604	−0.56	27	0.03	TP
1591	−0.59	27	0.03	TP
1590	−0.66	34	0.06	SP
1575	−0.65	37	0.05	SP
1571	−0.63	32	0.03	TP
1559	−0.72	38	0.05	SP
1542	−0.66	35	0.03	TP
1522	−0.65	34	0.03	TP
1515	−0.72	41	0.05	SP
1490	−0.67	30	0.03	TP
1488	−0.73	43	0.07	SP
1479	−0.74	42	0.05	SP
1467	−0.71	30	0.03	TP
1461	−0.76	39	0.06	SP
1447	−0.73	28	0.03	TP
1443	−0.78	32	0.06	SP
1416	−0.81	24	0.05	SP
1413	−0.82	25	0.03	TP
1392	−0.82	30	0.05	SP
1388	−0.84	34	0.03	TP
1362	−0.84	40	0.03	TP
1360	−0.87	38	0.06	SP
1345	−0.88	42	0.03	TP
1331	−0.93	37	0.05	SP
1307	−0.93	28	0.06	SP
1286	−0.97	46	0.03	TP
1284	−1.01	19	0.06	SP
1262	−0.99	22	0.05	SP
1261	−0.96	46	0.03	TP
1246	−1.03	26	0.06	SP
1243	−0.97	46	0.03	TP
1231	−1.04	30	0.05	SP
1215	−1.00	46	0.03	TP
1213	−1.11	35	0.06	SP
1200	−1.01	52	0.03	TP
1196	−1.14	38	0.05	SP
1184	−1.15	39	0.05	SP
1180	−1.05	59	0.03	TP
1167	−1.08	63	0.03	TP
1167	−1.15	39	0.06	SP
1152	−1.20	40	0.05	SP
1148	−1.08	68	0.03	TP
1131	−1.21	76	0.04	TP
1131	−1.23	40	0.06	SP
1119	−1.26	41	0.06	SP
1110	−1.23	96	0.03	TP
1097	−1.22	107	0.03	TP
1094	−1.29	40	0.05	SP
1077	−1.26	125	0.03	TP
1075	−1.32	40	0.06	SP
1058	−1.34	38	0.05	SP
1044	−1.23	153	0.03	TP
1040	−1.36	35	0.05	SP
1029	−1.39	32	0.05	SP
1025	−1.30	168	0.03	TP
1012	−1.30	179	0.03	TP
1006	−1.40	27	0.05	SP
992	−1.33	193	0.03	TP
979	−1.44	36	0.06	SP
966	−1.46	39	0.05	SP
932	−1.52	41	0.05	SP
889	−1.54	52	0.05	SP
862	−1.58	57	0.06	SP
845	−1.58	59	0.06	SP
821	−1.62	59	0.06	SP
804	−1.62	60	0.05	SP

North Carolina

Year (AD/BC)	RSL (m)	Age error (yrs)	RSL error (m)	Site
780	−1.66	58	0.05	SP
729	−1.72	56	0.06	SP
717	−1.73	58	0.06	SP
707	−1.70	60	0.04	SP
696	−1.71	61	0.04	SP
674	−1.76	62	0.04	SP
653	−1.85	61	0.04	SP
620	−1.89	56	0.05	SP
611	−1.87	54	0.05	SP
572	−1.91	46	0.06	SP
538	−1.86	50	0.06	SP
512	−1.96	52	0.04	SP
495	−1.94	52	0.05	SP
471	−1.98	48	0.06	SP
450	−2.05	48	0.07	SP
407	−2.02	56	0.05	SP
375	−2.14	59	0.05	SP
354	−2.06	59	0.05	SP
318	−2.16	58	0.05	SP
290	−2.19	62	0.05	SP
237	−2.22	68	0.06	SP
164	−2.28	69	0.05	SP
132	−2.28	65	0.06	SP
94	−2.41	60	0.06	SP
57	−2.42	63	0.06	SP
37	−2.42	65	0.09	SP
17	−2.42	67	0.07	SP
−3	−2.42	69	0.05	SP
−33	−2.50	68	0.06	SP
−84	−2.51	63	0.08	SP
−120	−2.55	59	0.08	SP

Massachusetts

Year (AD)	RSL (m)	Age Error (yrs)	RSL Error (m)
1963	−0.02	0	0.11
1930	−0.05	10	0.11
1875	−0.19	25	0.11
1700	−0.35	50	0.11
1669	−0.39	25	0.11
1600	−0.42	90	0.11
1487	−0.49	95	0.11
1486	−0.49	91	0.11
1415	−0.52	60	0.11
997	−0.59	68	0.11
941	−0.63	54	0.11
932	−0.64	100	0.11
728	−0.74	101	0.11
707	−0.84	96	0.11
671	−0.93	61	0.11
619	−0.98	40	0.11
507	−1.02	74	0.11
463	−1.12	78	0.11

Table S2. Fingerprints for North Carolina and other areas with proxy sea-level data

	Greenland (mm/yr)	Antarctica plus others (mm/yr)	Meier (mm/yr)	Sum (mm/yr)			
Wt *	0.54	0.99	0.46	1.99			
Wt †	0.60	0.61	0.46	1.67		Factors relative to NC	
				For wt *	For wt †	x NC (1)	x NC (2)
Nova Scotia	0.20	1.00	0.90	0.76	0.69	1.14	1.21
Massachusetts	0.30	1.00	0.90	0.79	0.72	1.10	1.15
Connecticut	0.40	1.00	0.90	0.81	0.76	1.07	1.09
North Carolina	0.60	1.00	0.90	0.87	0.83	1.00	1.00
Louisiana	0.80	1.00	0.95	0.93	0.91	0.93	0.91

*uses ice and Earth models (1)

†uses a modified GIA model, where lower mantle viscosity is increased from 2×10^{21} to 5×10^{21} Pa s, in order to better fit to tide gauges on the US Atlantic coast (1)

1 Mitrovica JX, Tamisiea ME, Davis JL, Milne GA (2001) Recent mass balance of polar ice sheets inferred from patterns of global sea-level change. *Nature* 409:1026–1029.

Table S3. Assumed prior statistics

Item	Distribution	Remarks
$T(t < \text{AD } 1850)$	$M(t) + N(0,(0.15\text{ K})^2)$	decadal, uncorrelated; (2)
$T(\text{AD}1850\text{–}1950)$	$M(t) + N(0,(0.06\text{ K})^2)$	decadal, uncorrelated; (3)
$T(\text{AD } 1950\text{–}2006)$	$M(t) + N(0,(0.04\text{ K})^2)$	decadal, uncorrelated; (3)
a	$N(0.56\text{ cm/yr/K},(0.05\text{ cm/yr/K})^2)$	(1)
$\langle T_0(\text{AD}1880\text{–}2000)\rangle$	$\langle T(\text{AD } 1951\text{–}1980)\rangle + N(-0.41\text{ K},(0.03\text{ K})^2)$	(1) constrained T_0 for this interval
a_1	$U(0.01,0.51)$ cm/yr/K	secular response part
b	$N(-4.9\text{ cm}/K,(1.0\text{ cm/K})^2)$	(1)
τ	$400 \bullet \exp(U(-2,2))$ yrs	$\ln(\tau)$ uniformly distributed for $\tau = 135\text{–}7400$ years
$T_0(\text{AD } 500)$	$N(\langle T(\text{AD } 500\text{–}700)\rangle,(0.2\text{ K})^2)$	starting value for T_0 integration
H_0	$C + U(-5,5)$ cm	sea-level integration constant

$M(t)$ refers to the proxy-reconstructed paleotemperatures used; C is a constant chosen for computational reasons such that the prior will not constrain the posterior. $N(\mu, \sigma^2)$ is the normal distribution of central value μ and variance σ^2; $U(a,b)$ is the uniform distribution between a and b. K is Kelvin

1 Rahmstorf S (2007) A semiempirical approach to projecting future sea-level rise. *Science* 315:368–370.
2 Mann ME, et al. (2008) Proxy-based reconstructions of hemispheric and global surface temperature variations over the past two millennia. *Proc Nat'l Acad Sci USA* 105:13252–13257.
3 Brohan P, Kennedy JJ, Harris I, Tett SFB, Jones PD (2006) Uncertainty estimates in regional and global observed temperature changes: a new dataset from 1850. *J Geophys Res* 111:D12106.